A&A 517, A65 (2010)
DOI: 10.1051/0004-6361/201014116

Astronomy & Astrophysics

Internal dynamics of Abell 2294: a massive, likely merging cluster

M. Girardi[1,2], W. Boschin[3], and R. Barrena[4,5]

[1] Dipartimento di Fisica dell' Università degli Studi di Trieste – Sezione di Astronomia, via Tiepolo 11, 34143 Trieste, Italy
e-mail: girardi@oats.inaf.it
[2] INAF – Osservatorio Astronomico di Trieste, via Tiepolo 11, 34143 Trieste, Italy
[3] Fundación Galileo Galilei – INAF, Rambla José Ana Fernández Perez 7, 38712 Breña Baja (La Palma), Canary Islands, Spain
[4] Instituto de Astrofísica de Canarias, C/Vía Láctea s/n, 38205 La Laguna (Tenerife), Canary Islands, Spain
[5] Departamento de Astrofísica, Universidad de La Laguna, Av. del Astrofísico Franciso Sánchez s/n, 38205 La Laguna (Tenerife), Canary Islands, Spain

Received 22 January 2010 / Accepted 18 April 2010

ABSTRACT

Context. The mechanisms giving rise to diffuse radio emission in galaxy clusters, and in particular their connection with cluster mergers, are still debated.
Aims. We seek to explore the internal dynamics of the cluster Abell 2294, which has been shown to host a radio halo.
Methods. Our analysis is mainly based on redshift data for 88 galaxies acquired at the Telescopio Nazionale Galileo. We combine galaxy velocities and positions to select 78 cluster galaxies and analyze its internal dynamics. We also use both photometric data acquired at the Isaac Newton Telescope and X-ray data from the Chandra archive.
Results. We re-estimate the redshift of the large, brightest cluster galaxy (BCG) obtaining $\langle z \rangle = 0.1690$, which closely agrees with the mean cluster redshift. We estimate a quite large line-of-sight (LOS) velocity dispersion $\sigma_V \sim 1400$ km s^{-1} and X-ray temperature $T_X \sim 10$ keV. Our optical and X-ray analyses detect substructure. Our results imply that the cluster is composed of two massive subclusters separated by a LOS rest frame velocity difference $V_{rf} \sim 2000$ km s^{-1}, very closely projected in the plane of sky along the SE-NW direction. This observational picture, interpreted in terms of the analytical two-body model, suggests that Abell 2294 is a cluster merger elongated mainly in the LOS direction and captured during the bound outgoing phase, a few fractions of Gyr after the core crossing. We find that Abell 2294 is a very massive cluster with a range of $M = 2{-}4 \times 10^{15}\ h_{70}^{-1}\ M_\odot$, depending on the adopted model. In contrast to previous findings, we find no evidence of Hα emission in the spectrum of the BCG galaxy.
Conclusions. The emerging picture of Abell 2294 is that of a massive, quite "normal" merging cluster, like many clusters hosting diffuse radio sources. However, perhaps because of its particular geometry, more data are needed for reach a definitive, more quantitative conclusion.

Key words. galaxies: clusters: individual: Abell 2294 – galaxies: clusters: general – galaxies: kinematics and dynamics

1. Introduction

Merging processes constitute an essential ingredient of the evolution of galaxy clusters (see Feretti et al. 2002b, for a review). An interesting aspect of these phenomena is the possible connection between cluster mergers and extended, diffuse radio sources: halos and relics. The synchrotron radio emission of these sources demonstrates the existence of large-scale cluster magnetic fields and of widespread relativistic particles. Cluster mergers have been proposed to provide the large amount of energy necessary for electron reacceleration to relativistic energies and for magnetic field amplification (Tribble 1993; Feretti 1999, 2002a; Sarazin 2002). Radio relics ("radio gischts" as referred to by Kempner et al. 2004), which are polarized and elongated radio sources located in the cluster peripheral regions, seem to be directly associated with merger shocks (e.g., Ensslin et al. 1998; Roettiger et al. 1999; Ensslin & Gopal-Krishna 2001; Hoeft et al. 2004). Radio halos, unpolarized sources that permeate the cluster volume in a similar way to the X-ray emitting gas (intracluster medium, hereafter ICM), are more likely to be associated with the turbulence following a cluster merger (Cassano & Brunetti 2005; Brunetti et al. 2009). However, the precise radio halos/relics formation scenario remains unclear because diffuse radio sources are quite uncommon and one has been able to study these phenomena only recently on the basis of a sufficient statistics (few dozen clusters up to $z \sim 0.3$, e.g., Giovannini et al. 1999; see also Giovannini & Feretti 2002; Feretti 2005; Giovannini et al. 2009) and attempt a classification (e.g., Kempner et al. 2004; Ferrari et al. 2008). It is expected that new telescopes will largely increase the statistics of diffuse sources (e.g., LOFAR, Cassano et al. 2009).

From the observational point of view, there is growing evidence of the connection between diffuse radio emission and cluster merging, since up to now diffuse radio sources have been detected only in merging systems. In several cases the cluster dynamical state has been derived from X-ray observations (see Buote 2002; Feretti 2008, 2006, and refs. therein). Optical data are a powerful way to investigate the presence and the dynamics of cluster mergers (e.g., Girardi & Biviano 2002), too. The spatial and kinematical analysis of member galaxies allow us to detect and measure the amount of substructure, and both identify and analyze possible pre-merging clumps or merger remnants. This optical information is really complementary to X-ray information since galaxies and the intra-cluster medium react on different timescales during a merger (see, e.g., numerical simulations by Roettiger et al. 1997).

In this context, we are conducting an intensive observational and data analysis program to study the internal dynamics of

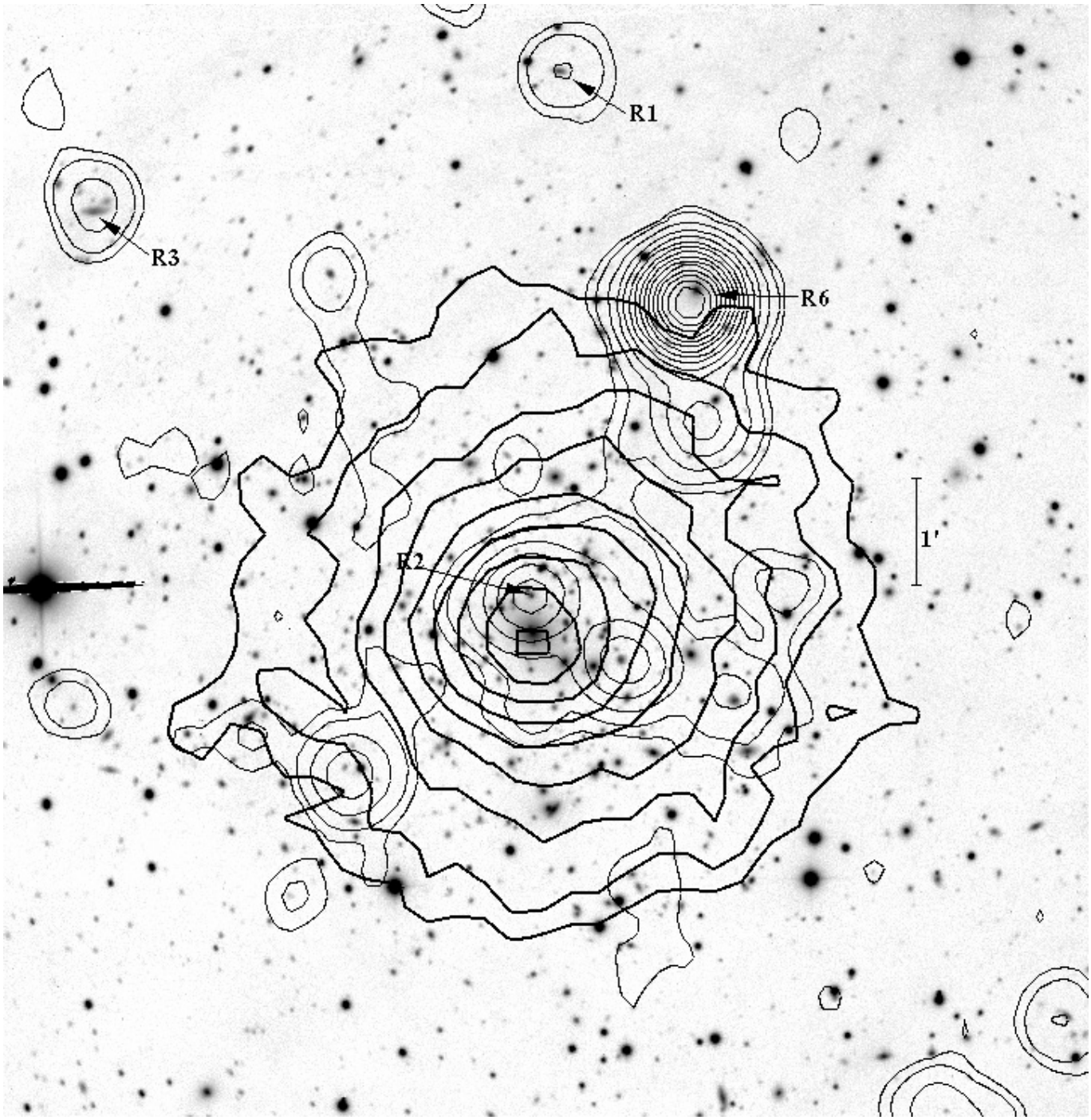

Fig. 1. INT *R*-band image of the cluster A2294 (north at the top and east to the left) with, superimposed, the contour levels of the Chandra archival image ID 3246 (thick contours; photons in the energy range 0.5–2 keV) and the contour levels of a VLA radio image at 1.4 GHz (thin contours, see Giovannini et al. 2009). Labels and arrows highlight the positions of radio sources listed by Rizza et al. (2003).

clusters with diffuse radio emission by using member galaxies (Girardi et al. 2007[1]). Most clusters exhibiting diffuse radio emission have a relatively high gravitational mass (higher than 0.7×10^{15} within 2 h_{70}^{-1} Mpc; see Giovannini & Feretti 2002) and, indeed, most clusters we analyzed are very massive clusters with few exceptions (Boschin et al. 2008).

During our observational program, we have conducted an intensive study of the cluster Abell 2294 (hereafter A2294). A2294 is a very rich, X-ray luminous, and hot Abell cluster: Abell richness class = 2 (Abell et al. 1989); $L_X(0.1–2.4\ \mathrm{keV}) = 6.6\times10^{44}\ h_{50}^{-2}\ \mathrm{erg\ s^{-1}}$; T_X = 8–9 keV recovered from ROSAT and Chandra data (Ebeling et al. 1998; Rizza et al. 1998; Maughan et al. 2008). Optically, the cluster is classified as Bautz-Morgan class II (Abell et al. 1989) and is dominated by a central, large brightest cluster galaxy (BCG, see Fig. 1).

According to both ROSAT and Chandra data, A2294 is known to have no cool core (Rizza et al. 1998; Bauer et al. 2005). As for the presence of possible substructure, using ROSAT data, Rizza et al. (1998) found evidence of a "centroid shift" and

[1] see also the web site of the DARC (Dynamical Analysis of Radio Clusters) project: http://adlibitum.oat.ts.astro.it/girardi/darc.

detected a southern excess in the X-ray emission. Using Chandra data, Hashimoto et al. (2007) classified A2294 as a "distorted" cluster because of the large value of its asymmetry parameter. Indeed, A2294 is a very peculiar cluster since, in contrast to the absence of a cooling core, it is very compact in its X-ray appearance (see Fig. 3 of Bauer et al. 2005). Among a sample of 115 clusters analyzed using Chandra data, A2294 has the smallest ellipticity, and exhibits a small, but highly significant, centroid shift (Maughan et al. 2008).

In another respect, A2294 is also peculiar. Out of a sample of 13 clusters at $z \sim 0.15-0.4$ showing evidence for Hα emission in their BCG spectrum, it is the only one that does not appear to have a cool core (see Fig. 5 of Bauer et al. 2005). The correlation between BCG Hα emission and the presence of a cool core is also found for nearby clusters where "Hα luminous galaxies lie at the center of large cool cores, although this special cluster environment does not guarantee the emission-line nebulosity in its BCG" (Peres et al. 1998). More recent observations also agree that Hα emission is more typical of cool core clusters than of non-cool core clusters (~70% compared to ~10%, Edwards et al. 2007).

As for the diffuse radio emission, Owen et al. (1999) first reported the existence of a detectable diffuse radio source in this cluster. Despite the presence of some disturbing point-like sources in the central region of the cluster, Giovannini et al. (2009) were able to detect a radio-halo 3′ in size. In particular, the position of A2294 in the $P_{1.4\,\mathrm{GHz}}$ (radio power at 1.4 GHz) – L_X plane is consistent with that of all other radio-halo clusters (see Fig. 17 of Giovannini et al. 2009).

To date, only a small amount of optical data have been available. The cluster redshift reported in the literature ($z = 0.178$) is based only on the BCG Hα emission line (Crawford et al. 1995). Instead, the true cluster redshift, as estimated in this paper, is rather $\langle z \rangle = 0.169$ fully consistent with that measured for the BCG on the basis of our data, which, indeed, do not show any evidence of Hα emission (see Sect. 2).

Our new spectroscopic and photometric data come from the Telescopio Nazionale Galileo (TNG) and the Isaac Newton Telescope (INT), respectively. Our present analysis is based on these optical data and X-ray Chandra archival data.

This paper is organized as follows. We present our new optical data and the cluster catalog in Sect. 2. We present our results about the cluster structure based on optical and X-ray data in Sects. 3 and 4, respectively. We briefly discuss our results and present our conclusions in Sect. 5.

Unless otherwise stated, we indicate errors at the 68% confidence level (hereafter c.l.). Throughout this paper, we use $H_0 = 70\ \mathrm{km\,s^{-1}\,Mpc^{-1}}$ in a flat cosmology with $\Omega_0 = 0.3$ and $\Omega_\Lambda = 0.7$. In the adopted cosmology, 1′ corresponds to $\sim 173\ h_{70}^{-1}$ kpc at the cluster redshift.

2. New data and galaxy catalog

Multi-object spectroscopic observations of A2294 were carried out at the TNG telescope in December 2007 and August 2008. We used DOLORES/MOS with the LR-B Grism 1, yielding a dispersion of 187 Å/mm. We used the new 2048 × 2048 pixels E2V CCD, with a pixel size of 13.5 μm. In total, we observed 4 MOS masks (3 in 2007 and 1 in 2008) for a total of 124 slits. We acquired three exposures of 1800 s for each mask. Wavelength calibration was performed using helium-argon lamps. Reduction of spectroscopic data was carried out using the IRAF[2] package. Radial velocities were determined using the cross-correlation technique (Tonry & Davis 1979) implemented in the RVSAO package (developed at the Smithsonian Astrophysical Observatory Telescope Data Center). Each spectrum was correlated against six templates for a variety of galaxy spectral types: E, S0, Sa, Sb, Sc, and Ir (Kennicutt 1992). The template producing the highest value of $\mathcal{R}$, i.e., the parameter given by RVSAO and related to the signal-to-noise ratio of the correlation peak, was chosen. Moreover, all spectra and their best correlation functions were examined visually to verify the redshift determination. In six cases (IDs. 5, 13, 15, 60, 81, and 82; see Table 1), we assumed the EMSAO redshift to be a reliable estimate of the redshift.

Our spectroscopic catalog lists 88 galaxies in the field of A2294.

The nominal errors as given by the cross-correlation are known to be smaller than the true errors (e.g., Malumuth et al. 1992; Bardelli et al. 1994; Ellingson & Yee 1994; Quintana et al. 2000). Duplicate observations for the same galaxy allowed us to estimate the true intrinsic errors in data of the same quality taken with the same instrument (e.g. Barrena et al. 2007a,b). Here we have a limited number of double determinations (i.e., five galaxies from four different masks), thus we decided to apply the correction that had already been applied in above studies. Hereafter we assume that true errors are larger than nominal cross-correlation errors by a factor of 1.4. For the five galaxies with two redshift estimates, we used the weighted mean of the two measurements and the corresponding errors. The median error in cz is 71 km s^{-1}.

Our photometric observations were carried out with the Wide Field Camera (WFC), mounted at the prime focus of the 2.5 m INT telescope. We observed A2294 in May 18th 2007 with filters B_H and R_H in photometric conditions and a seeing of ~1.5″.

The WFC consists of a four-CCD mosaic covering a 33′ × 33′ field of view, with only a 20% marginally vignetted area. We took nine exposures of 720 s in B_H and 360 s in R_H Harris filters (a total of 6480 s and 3240 s in each band) developing a dithering pattern of nine positions. This observing mode allowed us to build a "supersky" frame that was used to correct our images for fringing patterns (Gullixson 1992). In addition, the dithering helped us to clean cosmic rays and avoid the effects of gaps between the CCDs in the final images. Another problem associated with the wide field frames is the distortion of the field. To match the photometry of several filters, a good astrometric solution is needed to take into account these distortions. Using the *imcoords* IRAF tasks and taking as a reference the USNO B1.0 catalog, we were able to find an accurate astrometric solution (rms ~0.4″) across the full frame. The photometric calibration was performed by observing standard Landolt fields (Landolt 1992).

We finally identified galaxies in our B_H and R_H images and measured their magnitudes with the SExtractor package (Bertin & Arnouts 1996) and AUTOMAG procedure. In a few cases (e.g., close companion galaxies, galaxies close to defects of the CCD) the standard SExtractor photometric procedure failed. In these cases, we computed magnitudes by hand. This method consisted of assuming a galaxy profile of a typical elliptical galaxy and scaling it to the maximum observed value. The integration of this profile provided an estimate of the magnitude.

[2] IRAF is distributed by the National Optical Astronomy Observatories, which are operated by the Association of Universities for Research in Astronomy, Inc., under cooperative agreement with the National Science Foundation.

Table 1. Velocity catalog of 88 spectroscopically measured galaxies in the field of the cluster A2294.

ID	α, δ (J2000)	B	R	v (km s^{-1})	Δv	Emission lines
1	17 21 01.75 ,+85 51 21.1	18.65	17.21	28 640	57	
2	17 21 09.36 ,+85 53 32.7	19.79	17.82	51 333	67	
3	17 21 14.69 ,+85 57 31.3	19.04	16.92	52 128	55	
4	17 21 23.83 ,+85 54 29.0	20.24	18.17	51 318	77	
5	17 21 33.77 ,+85 56 33.5	20.29	19.42	48 560	16	[OII]
6	17 21 35.57 ,+85 53 21.4	20.89	18.88	50 550	71	
7	17 21 52.15 ,+85 53 53.1	19.92	18.05	52 312	59	
8	17 22 05.21 ,+85 56 42.0	20.75	19.10	50 779	147	
9	17 22 13.44 ,+85 56 40.9	19.86	17.83	52 063	59	
10	17 22 20.83 ,+85 50 54.7	19.42	18.19	36 167	77	
11	17 22 22.49 ,+85 52 05.8	18.51	17.21	50 279	109	
12	17 22 23.50 ,+85 54 14.6	20.77	18.81	50 787	66	
13	17 22 29.06 ,+85 52 33.8	18.49	17.68	53 150	75	[OII], Hβ
14	17 22 32.31 ,+85 55 59.5	20.97	18.83	51 408	112	
15	17 22 35.95 ,+85 48 54.6	18.56	17.22	21 565	109	Hα
16	17 22 37.99 ,+85 55 19.7	19.55	17.54	49 334	52	
17	17 22 47.69 ,+85 56 20.1	18.87	16.64	49 774	62	
18	17 22 51.26 ,+85 52 59.6	18.99	16.89	51 816	45	
19	17 22 56.69 ,+85 50 41.1	20.57	18.79	49 831	77	
20	17 23 08.14 ,+85 56 01.1	21.08	19.14	50 558	77	
21	17 23 10.54 ,+85 52 05.5	19.02	17.04	50 342	45	
22	17 23 15.98 ,+85 52 16.1	20.84	18.94	48 439	108	
23	17 23 23.83 ,+85 52 35.9	19.98	17.89	54 000	55	
24	17 23 26.93 ,+85 52 56.8	19.06	18.06	53 404	109	[OII], Hβ, Hα, [NII]
25	17 23 28.63 ,+85 52 00.2	19.92	17.97	52 231	60	
26	17 23 35.18 ,+85 53 13.3	20.05	17.97	50 231	54	
27	17 23 40.37 ,+85 51 54.6	19.16	17.36	50 708	66	
28	17 23 41.37 ,+85 52 53.2	18.76	16.64	49 068	34	
29	17 23 41.47 ,+85 53 50.2	19.54	17.60	48 114	64	
30	17 23 41.73 ,+85 54 43.2	19.97	17.91	52 330	48	
31	17 23 42.82 ,+85 55 01.1	20.22	18.09	47 906	70	
32	17 23 45.34 ,+85 53 55.6	19.33	17.39	49 027	52	
33	17 23 49.32 ,+85 50 37.0	20.67	18.87	51 693	113	
34	17 23 49.37 ,+85 50 39.7	20.12	18.50	53 475	57	
35	17 23 49.78 ,+85 49 38.1	20.67	18.70	52 794	99	
36	17 23 52.46 ,+85 51 01.1	20.48	18.41	53 149	59	
37	17 23 54.51 ,+85 49 53.6	20.17	18.34	50 294	77	
38	17 23 55.53 ,+85 53 17.8	19.82	17.92	51 367	104	
39	17 23 55.92 ,+85 52 55.7	18.67	16.76	49 221	41	
40	17 24 00.51 ,+85 53 43.4	20.52	18.44	52 927	78	
41	17 24 00.91 ,+85 54 37.6	19.09	17.10	46 553	60	
42	17 24 01.54 ,+85 51 34.3	18.16	17.18	52 055	31	
43	17 24 03.53 ,+85 51 34.7	19.26	17.80	49 876	69	
44	17 24 06.91 ,+85 51 44.7	20.41	18.19	51 991	69	
45	17 24 11.76 ,+85 50 03.4	20.91	19.00	51 059	133	
46	17 24 12.14 ,+85 53 12.0	17.12	15.01	50 671	66	
47	17 24 12.94 ,+85 53 32.4	20.02	18.05	48 983	71	
48	17 24 13.62 ,+85 53 14.7	20.03	17.86	51 068	186	
49	17 24 14.94 ,+85 53 35.1	20.34	18.58	50 477	101	
50	17 24 22.95 ,+85 52 00.0	20.06	18.12	52 427	97	
51	17 24 28.34 ,+85 53 25.9	19.69	17.61	49 638	63	
52	17 24 33.43 ,+85 53 25.5	21.04	18.95	50 207	74	
53	17 24 36.29 ,+85 52 57.0	20.72	18.58	49 332	88	
54	17 24 44.81 ,+85 54 44.7	19.57	17.57	51 597	76	
55	17 24 48.05 ,+85 53 05.9	20.52	18.68	48 339	76	
56	17 24 54.51 ,+85 53 53.1	20.52	18.45	49 696	70	
57	17 24 55.99 ,+85 52 11.3	19.92	17.84	49 614	85	
58	17 24 59.28 ,+85 52 44.2	20.67	18.67	49 486	56	
59	17 25 03.41 ,+85 50 25.1	20.52	18.42	52 052	74	
60	17 25 09.21 ,+85 50 16.9	21.11	20.61	67 190	313	[OII], Hβ, [OIII]
61	17 25 09.98 ,+85 54 10.7	21.77	19.77	49 754	104	
62	17 25 10.31 ,+85 50 15.0	20.77	18.77	51 675	218	
63	17 25 15.91 ,+85 53 33.0	19.87	19.02	53 186	66	
64	17 25 19.18 ,+85 53 26.5	20.20	18.21	49 892	116	
65	17 25 19.99 ,+85 55 54.0	20.51	18.71	51 267	113	
66	17 25 22.27 ,+85 52 52.7	20.31	18.92	146 216	80	
67	17 25 31.13 ,+85 53 44.8	20.58	18.69	51 558	57	
68	17 25 34.97 ,+85 55 48.5	20.78	18.84	51 215	67	
69	17 25 42.63 ,+85 51 27.3	20.08	18.04	52 589	70	
70	17 25 45.98 ,+85 55 53.9	19.95	18.29	58 151	92	[OII]
71	17 25 46.11 ,+85 53 44.3	21.58	19.96	81 954	294	
72	17 25 50.09 ,+85 51 43.2	20.54	18.58	52 040	49	
73	17 25 53.45 ,+85 56 55.0	19.77	18.66	48 662	85	[OII], Hβ
74	17 25 57.79 ,+85 56 29.1	19.54	18.27	57 854	111	[OII], Hβ
75	17 26 10.20 ,+85 54 35.9	19.31	17.25	50 852	48	
76	17 26 14.14 ,+85 52 19.3	20.50	18.59	50 445	66	
77	17 26 26.37 ,+85 54 27.9	19.78	17.83	51 769	80	
78	17 26 34.30 ,+85 52 58.7	20.37	18.76	47 581	87	
79	17 26 36.99 ,+85 52 23.7	18.83	17.04	49 923	60	
80	17 26 41.11 ,+85 53 38.2	19.93	18.02	49 484	64	
81	17 26 44.04 ,+85 56 58.2	21.52	19.85	89 709	18	[OII]
82	17 26 45.34 ,+85 51 21.5	19.95	18.93	49 890	64	[OII], Hβ, [OIII],Hα
83	17 26 50.47 ,+85 51 47.5	20.52	18.71	49 422	71	
84	17 26 58.03 ,+85 54 19.1	20.69	18.93	52 827	97	
85	17 27 08.45 ,+85 52 14.8	20.66	18.60	51 085	104	
86	17 27 08.50 ,+85 54 29.4	19.54	17.99	48 738	83	
87	17 27 22.08 ,+85 53 56.5	20.38	18.82	52 246	97	
88	17 27 35.04 ,+85 54 08.7	21.18	18.98	90 810	92	

Notes. ID 46, in boldface highlights the BCG. IDs in italics are non-member galaxies.

This method is similar to PSF photometry, but assumes a galaxy profile, which is more appropriate in this case.

We transformed all magnitudes into the Johnson-Cousins system (Johnson & Morgan 1953; Cousins 1976). We used $B = B_{\rm H} + 0.13$ and $R = R_{\rm H}$ as derived from the Harris filter characterization[3] and assuming a $B - V \sim 1.0$ for E-type galaxies (Poggianti 1997). As a final step, we estimated and corrected the Galactic extinction $A_B \sim 0.93$, $A_R \sim 0.58$ using Burstein & Heiles's (1982) reddening maps. These values are especially high because A2294 is immersed in a diffuse dust cloud soaring high above the plane of our Milky Way Galaxy, and known as the Polaris Dust Nebula. We estimated that our photometric sample is complete down to $R = 22.0$ (23.0) and $B = 23.5$ (24.5) for $S/N = 5$ (3) within the observed field.

We assigned magnitudes to all galaxies of our spectroscopic catalog. Table 1 lists the velocity catalog (see also Fig. 2): identification number of each galaxy, ID (Col. 1); right ascension and declination, α and δ (J2000, Col. 2); B and R magnitudes (Cols. 3 and 4); heliocentric radial velocities, $v = cz_\odot$ (Col. 5) with errors, Δv (Col. 6); and emission lines detected in the spectra (Col. 7).

The brightest galaxy of A2294 (ID. 46 in Table 1, hereafter BCG) is probably the dominant galaxy, 1.6 R-magnitudes more luminous than other cluster members. The measured redshift is $z = 0.1690 \pm 0.0002$, different from that reported by Crawford et al. (1995), $z = 0.178$, using INT data and measured on the Hα emission line only. This discrepancy prompted us to acquire additional data for this galaxy. In August 2009, we acquired two 900 s exposure long-slit spectra of the BCG. We used the LR-R

[3] we refer to http://www.ast.cam.ac.uk/~wfcsur/technical/photom/colours/

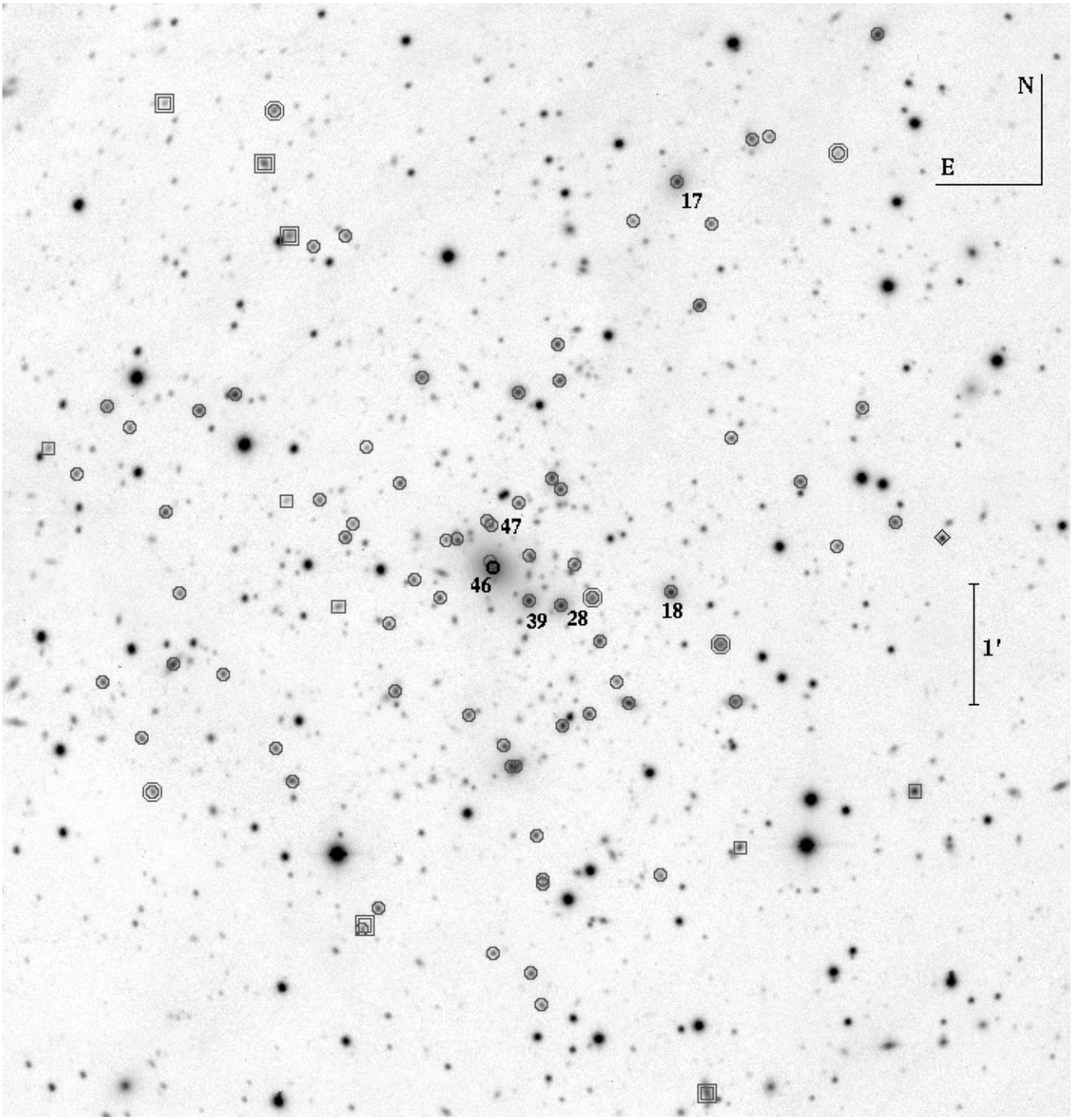

Fig. 2. INT *R*-band image of the cluster A2294 (north at the top and east to the left). Circles and squares indicate cluster members and non-members, respectively (see Table 1). Solid circle in the center highlights the position of the BCG galaxy. Annuli and box annuli show member and non-member emission line galaxies, respectively. Labels indicate the IDs of cluster galaxies cited in the text. A diamond at the right border of the image highlights a QSO at $z \sim 2.1$.

grism, covering the wavelength range ~4500–10 000 Å. The target was positioned in two slightly different positions along the slit to perform an optimal sky subtraction with a technique commonly used to reduce spectroscopic data in the near-infrared. Our reduced spectrum (see Fig. 3) does not show any evidence of the Hα emission. We note that the Hα emission reported by Crawford et al. (1995) is very strong $EW_{\rm H\alpha} = 51.7 \pm 3.2$ (see for comparison the spectrum of A291 having $EW_{\rm H\alpha} = 20.9 \pm 0.9$ in their Fig. 1) and thus its presence would be just striking in our spectrum. Indeed, we strongly suspect that their detection is caused by some problem in data reduction, e.g., a cosmic ray or sky subtraction, as also suggested by the incorrect measure of the galaxy redshift.

Other cluster members are far less luminous than the BCG: the brightest ones lie in the central cluster region (IDs. 28, 39 and 18) with the exception of ID. 17 (hereafter R6) which lies in the northern region and is very radio luminous ($>10^{24}$ W Hz^{-1}, No. 6 of Rizza et al. 2003). Out of radio galaxies listed

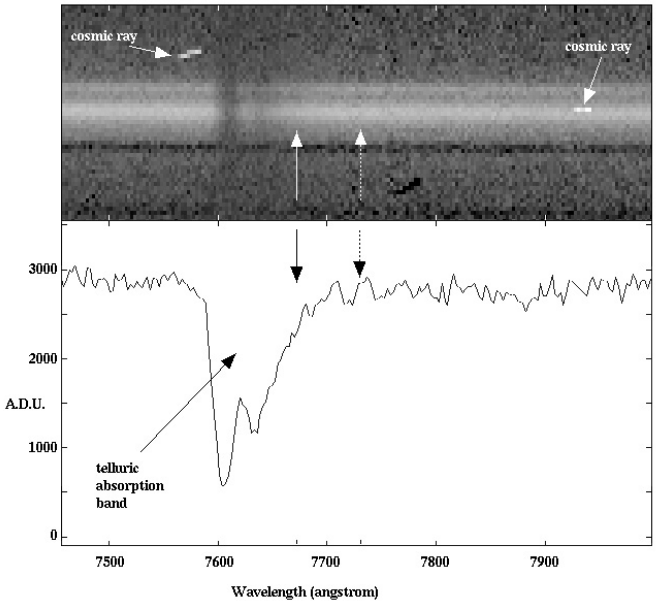

Fig. 3. *Top panel*: 2D spectrum of the BCG galaxy taken with the grism LR-R mounted on DOLORES in the wavelength range ~7500–8000 Å. *Bottom panel*: 1D reduced spectrum of the BCG galaxy in the same wavelength range as above. Solid and dashed arrows indicate the position of the (hypothetical) Hα emission line according to the redshift given in this paper and to the redshift provided by Crawford et al. (1995), respectively. The spectrum does not show any evidence of the Hα emission.

by Rizza et al. (2003), we also acquired a redshift for their No. 2 (ID. 47, labelled as R2 in Fig. 1), confirming its membership to the cluster.

3. Analysis of the spectroscopic sample

3.1. Member selection

To select cluster members among the 88 galaxies with redshifts, we follow a two-step procedure. We first perform the 1D adaptive-kernel method (hereafter DEDICA, Pisani 1993, 1996; see also Fadda et al. 1996; Girardi et al. 1996). We search for significant peaks in the velocity distribution at >99% c.l. This procedure detects A2294 as a peak at $z \sim 0.169$ populated by 80 galaxies considered as candidate cluster members (in the range $46\,553 \leq v \leq 58\,151$ km s^{-1}, see Fig. 4). Out of eight non-members, three and five are foreground and background galaxies, respectively.

All the galaxies assigned to the cluster peak are analyzed in the second step, which uses the combination of position and velocity information, i.e., the "shifting gapper" method by Fadda et al. (1996). This procedure rejects galaxies that are too far in velocity from the main body of galaxies within a fixed bin that shifts along the distance from the cluster center. The procedure is iterated until the number of cluster members converges to a stable value. Following Fadda et al. (1996), we use a gap of 1000 km s^{-1} – in the cluster rest-frame – and a bin of 0.6 h_{70}^{-1} Mpc, or large enough to include 15 galaxies. As for the center of A2294, we adopt the position of the BCG [RA = $17^{\rm h}24^{\rm m}12\overset{\rm s}{.}14$, Dec = $+85°53'12''$ (J2000.0)], which is almost coincident with the X-ray centroid obtained in this paper using Chandra data (see Sect. 4). The "shifting gapper" procedure rejects another two obvious interlopers very far from the main body (>2000 km s^{-1}) but that survived the first step of our member selection procedure. We obtain a sample of 78 fiducial members (see Fig. 5).

The five member galaxies exhibiting emission lines (ELGs) are preferentially found in the external cluster regions (see Fig. 2). The only ELG close to the cluster center (ID. 24) lies in the high tail of the velocity distribution, far more than $cz = 2500$ km s^{-1} from the mean cluster velocity, as expected e.g., in the case of a very radial orbit. These findings are in general agreement with large statistical analyses of ELGs in clusters (see Biviano et al. 1997, and refs. therein).

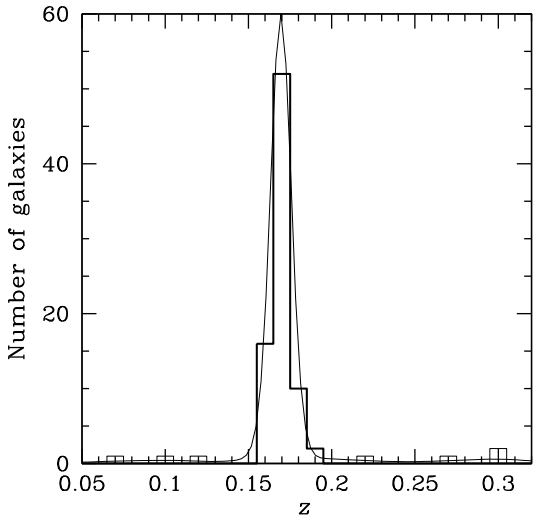

Fig. 4. Redshift galaxy distribution. The solid line histogram refers to the 80 galaxies assigned to the A2294 complex according to the DEDICA reconstruction method. The number-galaxy density in the redshift space, as provided by the adaptive kernel reconstruction method is superimposed on the histogram.

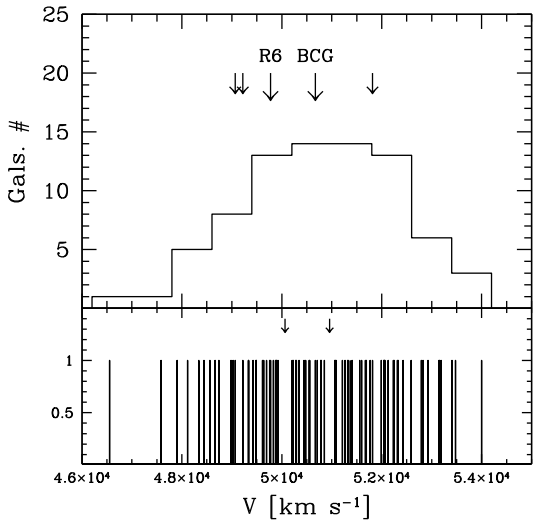

Fig. 5. The 78 galaxies assigned to the cluster. *Upper panel*: velocity distribution. The arrows indicate the velocities of the five brightest galaxies, in particular we indicate the brightest cluster galaxy "BCG", the bright radio galaxy "R6". *Lower panel*: stripe density plot where the arrows indicate the positions of the significant gaps.

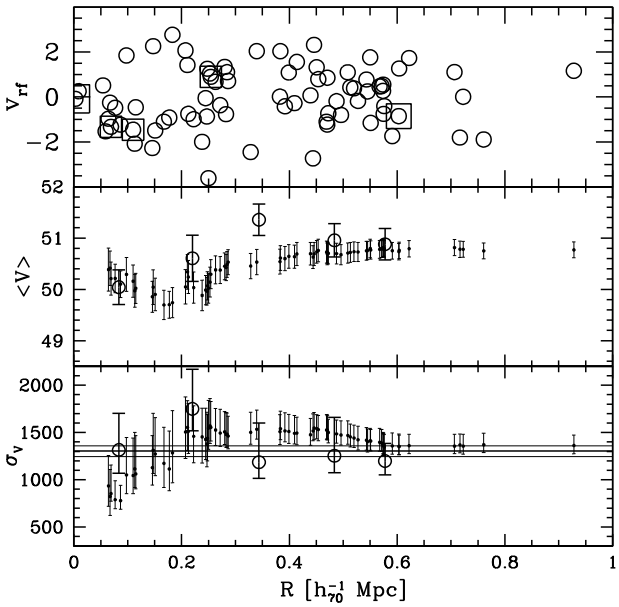

Fig. 6. *Top panel*: rest-frame velocity vs. projected distance from the cluster center. Squares indicate the five brightest galaxies. *Middle and bottom panels*: differential (big circles) and integral (small points) profiles of mean velocity and LOS velocity dispersion, respectively. For the differential profiles, we plot the values for five annuli from the center of the cluster, each of 0.25 h_{70}^{-1} Mpc (large symbols). For the integral profiles, the mean and dispersion at a given (projected) radius from the cluster-center is estimated by considering all galaxies within that radius – the first value computed on the five galaxies closest to the center. The error bands at the 68% c.l. are also shown. In the *lower panel*, the horizontal line represents the X-ray temperature (see Sect. 4) with the respective errors transformed in σ_V assuming the density-energy equipartition between ICM and galaxies, i.e. $\beta_{\rm spec} = 1$ (see Sect. 5).

3.2. Global cluster properties

By applying the biweight estimator to the 78 cluster members (Beers et al. 1990, ROSTAT software), we compute a mean cluster redshift of $\langle z \rangle = 0.1693 \pm 0.0005$, i.e. $\langle v \rangle = (50\,769 \pm 155)$ km s^{-1}. We estimate the LOS velocity dispersion, σ_V, by using the biweight estimator and applying the cosmological correction and the standard correction for velocity errors (Danese et al. 1980). We obtain $\sigma_{\rm V} = 1363^{+110}_{-91}$ km s^{-1}, where errors are estimated through a bootstrap technique.

To evaluate the robustness of the $\sigma_{\rm V}$ estimate, we analyze the velocity dispersion profile (Fig. 6). The integral profile rises out to $\sim 0.2\ h_{70}^{-1}$ Mpc and then flattens suggesting that a robust value of $\sigma_{\rm V}$ is asymptotically reached in the external cluster regions, as found for most nearby clusters (e.g., Fadda et al. 1996; Girardi et al. 1996).

In the framework of usual assumptions (cluster sphericity, dynamical equilibrium, coincidence of the galaxy and mass distributions), one can compute virial global quantities. Following the prescriptions of Girardi & Mezzetti (2001), we assume for the radius of the quasi-virialized region is $R_{\rm vir} = 0.17 \times \sigma_V / H(z) = 3.05\ h_{70}^{-1}$ Mpc from their Eq. (1) with the scaling of $H(z)$ (see also Eq. 8 of Carlberg et al. 1997 for R_{200}). We compute the virial mass (Limber & Mathews 1960; see also, e.g., Girardi et al. 1998)

$$M = 3\pi/2 \cdot \sigma_V^2 R_{\rm PV}/G - {\rm SPT}, \quad (1)$$

where SPT is the surface pressure term correction (The & White 1986) and $R_{\rm PV}$ is a projected radius (equal to two times the projected harmonic radius).

The estimate of σ_V is robust when computed within a large cluster region (see Fig. 6). The value of $R_{\rm PV}$ depends on the size of the sampled region and possibly on the quality of the spatial sampling (e.g., whether the cluster is uniformly sampled or not). Since in A2294 we sampled only a fraction of $R_{\rm vir}$, we have to use an alternative estimate of $R_{\rm PV}$ on the basis of the knowledge of the galaxy distribution. Following Girardi et al. (1998; see also Girardi & Mezzetti 2001), we assume a King-like distribution with parameters typical of nearby/medium-redshift clusters: a core radius $R_{\rm c} = 1/20 \times R_{\rm vir}$ and a slope-parameter $\beta_{\rm fit,gal} = 0.8$, i.e. the volume galaxy density at large radii goes as $r^{-3\beta_{fit,gal}} = r^{-2.4}$. We obtain $R_{\rm PV}(<R_{\rm vir}) = 2.27\ h_{70}^{-1}$ Mpc, where a 25% error is expected (Girardi et al. 1998, see also the approximation given by their Eq. (13) when $A = R_{\rm vir}$). The value of SPT depends strongly on the radial component of the velocity dispersion at the radius of the sampled region and could be obtained by analyzing the (differential) velocity dispersion profile, although this procedure would require several hundreds of galaxies. We decide to assume a 20% SPT correction as obtained in the literature by combining data on many clusters sampled out to about $R_{\rm vir}$ (Carlberg et al. 1997; Girardi et al. 1998). We compute $M(<R_{\rm vir} = 3.05\ h_{70}^{-1}$ Mpc$) = 3.7^{+1.1}_{-1.0} \times 10^{15}\ h_{70}^{-1}\ M_\odot$.

3.3. Velocity distribution

We analyze the velocity distribution to search for possible deviations from Gaussianity that might provide important signatures of complex dynamics. For the following tests, the null hypothesis is that the velocity distribution is a single Gaussian.

We estimate three shape estimators, i.e., the kurtosis, the skewness, and the scaled tail index (see, e.g., Bird & Beers 1993). We find no evidence that the velocity distribution departs from Gaussianity.

We then investigate the presence of gaps in the velocity distribution. We follow the weighted gap analysis presented by Beers et al. (1991, 1992; ROSTAT software). We look for normalized gaps larger than 2.25 since in random draws of a Gaussian distribution they arise at most in about 3% of the cases, independent of the sample size (Wainer & Schacht 1978). We detect two significant gaps (at the 97% and 98.6% c.l.s), which divide the cluster into three groups of 28, 14, and 36 galaxies from low to high velocities (hereafter GV1, GV2, and GV3, see Fig. 5). The BCG is assigned to the GV2 peak. Among other luminous galaxies, three galaxies (R6, ID. 28, and ID. 39) are assigned to the GV1 peak and one galaxy (ID. 18) is assigned to the GV3 peak.

Following Ashman et al. (1994), we also apply the Kaye's mixture model (KMM) algorithm. This test does not find a three-groups partition, which provides a significantly more accurate description of the velocity distribution than a single Gaussian.

3.4. 3D-analysis

The existence of correlations between positions and velocities of cluster galaxies is a characteristic of true substructures. Here we use three different approaches to analyze the structure of A2294 combining position and velocity information.

To search for a possible physical meaning of the three subclusters determined by the two weighted gaps, we compare two by two the spatial galaxy distributions of GV1, GV2, and GV3.

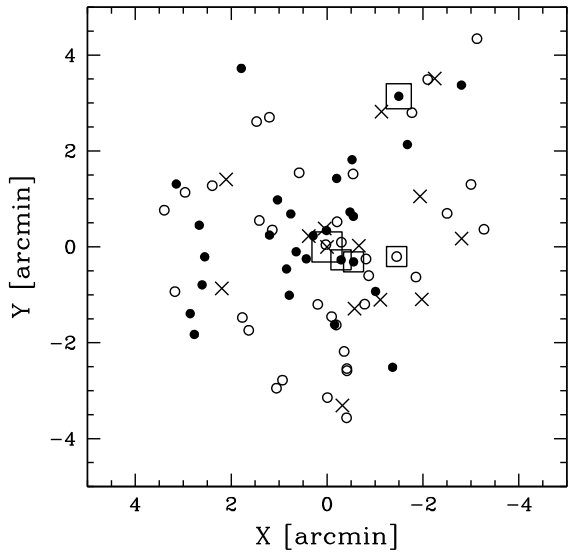

Fig. 7. Spatial distribution on the sky of the cluster galaxies showing the three groups recovered by the weighted gap analysis. Solid circles, crosses, and open circles indicate the galaxies of GV1, GV2, and GV3, respectively. The BCG is taken as the cluster center. Large squares indicate the five brightest cluster members. Among them, the BCG and R6 are indicated by the two largest squares.

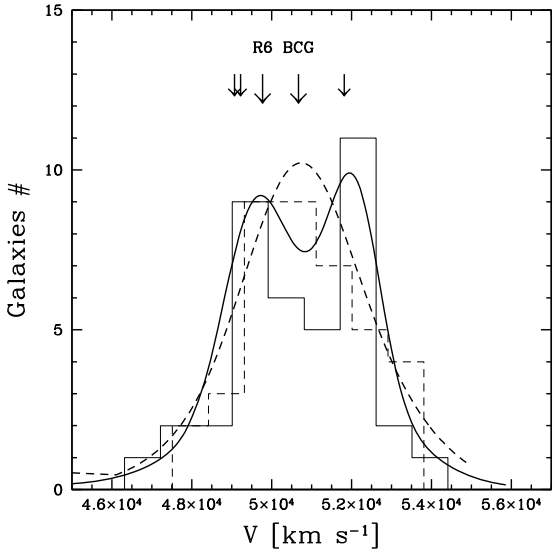

Fig. 8. Velocity galaxy distribution of more and less luminous cluster members (solid and dashed lines, respectively). The arrows indicate the velocities of the five brightest galaxies, in particular "BCG" indicates the bright, central galaxy and "R6" indicates the bright radio-galaxy. The number-galaxy densities, as provided by the adaptive kernel reconstruction method are superimposed on the histograms.

We find that the GV1 and GV3 groups differ in the distributions of the clustercentric distances of member galaxies at the 93% c.l. (according to the the 1D Kolmogorov-Smirnov test; hereafter 1DKS-test, see e.g., Press et al. 1992). The GV1 galaxies are, on average, closer to the cluster center than the GV3 galaxies (see Fig. 7).

We analyze the presence of a velocity gradient performing a multiple linear regression fit to the observed velocities with respect to the galaxy positions in the plane of the sky (e.g., Boschin et al. 2004, and refs. therein). We find a position angle on the celestial sphere of PA $= 214^{+33}_{-28}$ degrees (measured counter-clock wise from north), i.e. higher-velocity galaxies lie in the SSW region of the cluster. To assess the significance of this velocity gradient, we perform 1000 Monte Carlo simulations by randomly shuffling the galaxy velocities and for each simulation we determine the coefficient of multiple determination (RC^2, see e.g., NAG Fortran Workstation Handbook 1986). We define the significance of the velocity gradient as the fraction of times in which the RC^2 of the simulated data is smaller than the observed RC^2. We find that the velocity gradient is marginally significant at the 91% c.l.

We also combine galaxy velocity and position information to compute the Δ-statistics devised by Dressler & Schectman (1988; see also e.g., Boschin et al. 2006, for a recent application). We find no significant indication of substructure.

3.5. Kinematics of more luminous galaxies

The presence of velocity segregation of galaxies with respect to their colors, luminosities, and morphologies is often taken as evidence of advanced dynamical evolution of the parent cluster (e.g. Biviano et al. 1992; Fusco-Femiano & Menci 1998). Here we check for possible luminosity segregation of galaxies in the velocity space.

We find no significant correlation between the absolute velocity $|v|$ and R-magnitude. We also divide the sample into a low and a high-luminosity subsamples by using the median R-magnitude =18.145. The two subsamples do not differ in their velocity distribution as we verify with the standard means-test and F-test (e.g., Press et al. 1992) applied to the means and variances of velocities and with the 1DKS-test applied to the whole velocity distributions. This agrees with the very small range of action of velocity segregation in galaxy clusters, i.e. typically only the three most luminous galaxies (Biviano et al. 1992; see also Goto 2005).

Examining the velocity distributions of the two subsamples in more detail, we find that the distribution of luminous galaxies is found to be non-Gaussian according to the scale tail index (at the 95% c.l.) and that, according to the 1D-DEDICA technique, it is more accurately described by a bimodal distribution (see Fig. 8). The two peaks of this distribution, of 20 and 19 galaxies at ~49 700 and 51 950 km s^{-1} respectively, are separated by ~2000 km s^{-1} in the rest cluster frame and appear to overlap, i.e. 15 galaxies have a non-null probability of belonging to both the peaks. The BCG is assigned to the low-velocity peak, but has a high probability of belonging to the other peak. Among other luminous galaxies, R6, IDs. 28 and 39 are assigned to the low-velocity peak and ID. 18 to the high-velocity peak.

According to the DEDICA assignment, we estimate $\sigma_V \sim$ 780 and ~640 km s^{-1} for the low and high-velocity groups, respectively. However, since there is a wide velocity-range where galaxies have a non-zero probability of belonging to both the clumps, DEDICA membership assignment leads to an artificial truncation of the tails of the distributions. This truncation may lead to an underestimate of velocity dispersion for the subclusters. Thus, we prefer to rely on the estimates obtained through the KMM approach even if the tightest bimodal fit does not represent a significant improvement on that of the single Gaussian according to the likelihood ratio test. The low- and high-velocity

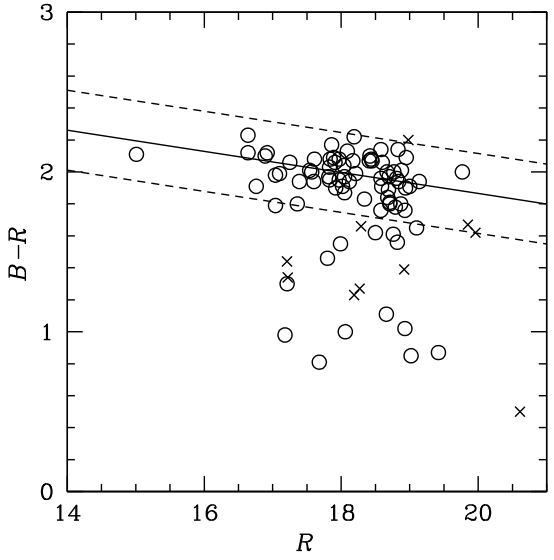

Fig. 9. *B–R* vs. *R* diagram for galaxies with available spectroscopy is shown by circles and crosses (cluster and field members, respectively). The solid line gives the best-fit color-magnitude relation as determined for member galaxies; the dashed lines are drawn at ±0.25 mag from the CMR.

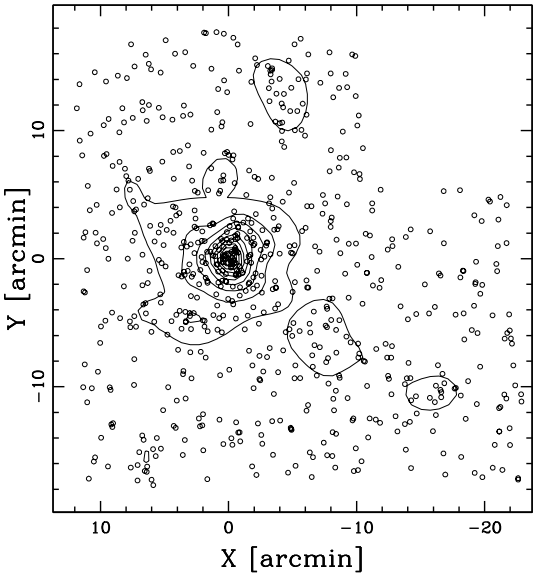

Fig. 10. Spatial distribution on the sky and relative isodensity contour map of likely cluster members extracted from our photometric catalog with $R \leq 21$. The contour map is obtained with the DEDICA method (black lines). The plot is centered on the cluster center.

groups given by the best KMM bimodal fit have mean velocities $\langle v \rangle \sim 49\,740$ and $52\,230$ km s^{-1}, in good agreement with the peak velocities reported above and $\sigma_V \sim 1070$ and ~670 km s^{-1}.

3.6. Analysis of the photometric sample

By applying the 2D adaptive-kernel method to the positions of A2294 galaxy members, we identify only one significant peak. However, our spectroscopic data do not cover the entire cluster field and are affected by magnitude incompleteness. To overcome these problems, from our photometric catalog we select likely members on the basis of the color-magnitude relation (hereafter CMR), which indicates the early-type galaxy locus. To determine the CMR, we fix the slope according to López-Cruz et al. (2004, see their Fig. 3) and apply the two-sigma-clipping fitting procedure to the cluster members obtaining $B–R = 3.185–0.066 \times R$ (see Fig. 9). From our photometric catalog, we consider as likely cluster members those objects with a SExtractor stellar index ≤0.9 lying within 0.25 mag of the CMR. To avoid contamination by field galaxies, we do not show results for galaxies fainter than 21 mag (in *R*-band). Figure 10 shows the contour map for the likely cluster members with $R \leq 21$: we find again that A2294 is well described by only one peak centered on the BCG galaxy.

4. X-ray analysis

The X-ray analysis of A2294 is performed on the archival data of the Chandra ACIS-I observation 800 246 (exposure ID #3246). The pointing has an exposure time of 10 ks. Data reduction is performed using the package CIAO[4] (Chandra Interactive Analysis of Observations, ver. 3.3 with CALDB ver. 3.2.1) on chips I0, I1, I2, and I3 (field of view ~17′ × 17′). First, we remove events from the level 2 event list with a status not equal to zero and with grades one, five, and seven. Then, we select all events with energy between 0.3 and 10 keV. In addition, we clean bad offsets and examine the data, filtering out bad columns and removing times when the count rate exceeds three standard deviations from the mean count rate per 3.3 s interval. We then clean the four chips for flickering pixels, i.e., times where a pixel has events in two sequential 3.3 s intervals. The resulting exposure time for the reduced data is 9.9 ks.

A quick look at the reduced image is sufficient to reveal the regular morphology of the extended X-ray emission of this cluster (see Fig. 11). The low values of the P_m/P_0 power ratios found by Bauer et al. (2005) quantitatively support this feeling. The absence of multiple clumps in the ICM is confirmed by performing a wavelet multiscale analysis on the chip I3: the task CIAO/Wavdetect identifies A2294 as a single extended X-ray source.

To more accurately characterize the X-ray morphology of the cluster, by using the CIAO package Sherpa we fit a simple Beta model to the 2D X-ray photon distribution on the chip I3. The model is defined to be (Cavaliere & Fusco-Femiano 1976)

$$S(R) = S_0[1 + (R/R_c)^2]^{\alpha} + b, \quad (2)$$

where R is the projected radial coordinate from the centroid position and b the surface brightness background level. Before the fit, we bin the image by a factor 8 and divide it by a normalized exposure map. The best-fit centroid position is located at RA = $17^h24^m04\overset{s}{.}87$ and Dec = +85°53′15.6″ (J2000.0, with an error of ±0.8″) at ~8.5″ from the position of the BCG. The slope parameter is $\alpha = -0.96 \pm 0.05$, that is $\beta_{\rm fit,\,gas} = (-\alpha + 0.5)/3 = 0.49 \pm 0.02$, and the (angular) core radius is $R_c = 36.2'' \,^{+2.7''}_{-2.5''}$. At the redshift of A2294, the core radius corresponds to $104.4^{+7.7}_{-7.3}\, h_{70}^{-1}$ kpc.

The above model provides an adequate description fit to the data (the reduced CSTAT statistic is 1.04; Cash 1979). However, we check for possible departures of the X-ray surface brightness, and thus of the gas density distribution, from the Beta model fit by investigating the Beta model residuals. The residuals show a

[4] CIAO is freely available at http://asc.harvard.edu/ciao/

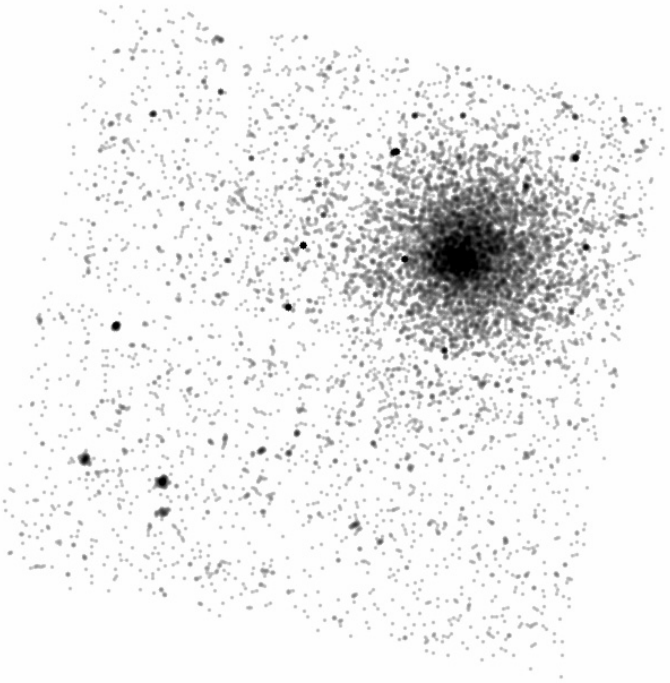

Fig. 11. 17′ × 17′ Chandra X-ray smoothed image (ID 3246) of A2294 in the energy band 0.5–2 keV (North at the top and East to the left).

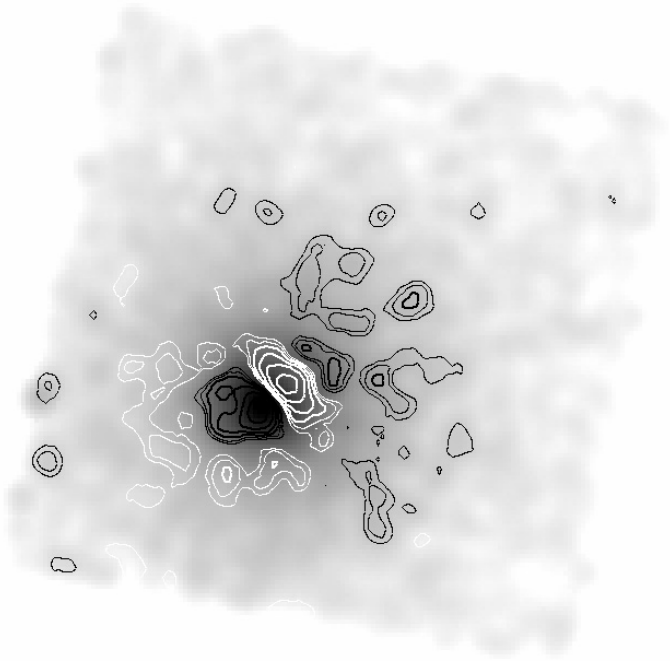

Fig. 12. The smoothed X-ray emission in the right-upper quadrant of Fig. 11 with, superimposed, the contour levels of the positive (black) and negative (white) smoothed Beta model residuals (North at the top and East to the left).

deficit of X-ray emitting gas in a region extending along the NE–SW direction, with a negative peak in the very central cluster region (see Fig. 12). Around the cluster center, elongated in the direction SE–NW, there are also regions that have an excess of positive residuals.

As for the spectral properties of the cluster X-ray photons, we compute a global estimate of the ICM temperature. The

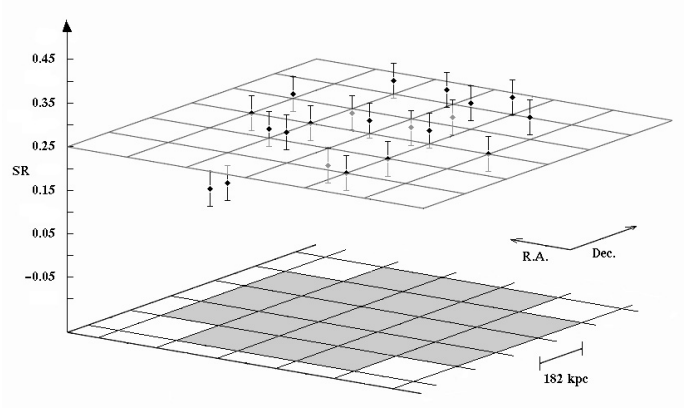

Fig. 13. Softness ratio 3D map of A2294 around the centroid of the X-ray distribution. The plane at the median SR value (0.25) is drawn.

temperature is computed from the X-ray spectrum of the cluster within a circular aperture of ∼173″ radius (0.5 h_{70}^{-1} Mpc at the cluster redshift) around the centroid of the X-ray emission. Fixing the absorbing galactic hydrogen column density at 6.19×10^{20} cm^{-2}, computed from the HI maps by Dickey & Lockman (1990), we fit a Raymond-Smith (1977) spectrum using the CIAO package Sherpa with a χ^2 statistics and assuming a metal abundance of 0.3 in solar units. We find a best-fit temperature of $T_X = 10.3 \pm 1.1$ keV.

A detailed temperature and metallicity map would be highly desirable to more accurately describe the properties of the ICM, but due to the relatively low exposure times, the photon statistics are insufficient for this aim. However, in a low signal-to-noise situation, possible temperature gradients in the ICM might be detected using the "hardness" (or "softness") map of the cluster. We create two images in the energy bands 0.5–2 keV (soft band) and 2–7 keV (hard band), subtracting a constant background level in each energy band. Computing counts in the soft (S) and in the hard (H) band, we define the quantity "softness ratio" as $SR = (S - H)/(S + H)$. Both images are exposure-corrected with their corresponding exposure maps. Because of the low number of photons available, we have to choose a large pixel size to obtain a high quality count statistic per pixel, so the resolution of the soft and hard images is low (182 kpc pix^{-1}). A 3D graph of the SR values in the pixels within a radius of 0.5 h_{70}^{-1} Mpc from the cluster center is reported in Fig. 13. Typical errors are ±0.4, while the median value of SR is 0.25. According to the PIMMS tool, this value corresponds to a temperature of ∼9.7 keV, in good agreement with the global temperature reported above. The SR 3D graph does not show any evidence of significant temperature gradients.

5. Discussion and conclusions

Our estimate of the cluster redshift is $\langle z \rangle = 0.1693 \pm 0.0005$ and the BCG is well at rest within the cluster (cf. our $z = 0.1690$ with $z = 0.178$ by Crawford et al. 1995).

For the first time, the internal dynamics of A2294 have been analyzed.

The high values of the velocity dispersion $\sigma_V = 1363^{+110}_{-91}$ km s^{-1} and X-ray temperature $T_X = (10.3 \pm 1.1)$ keV are comparable to the highest values found in typical clusters (see Mushotzky & Scharf 1997; Girardi & Mezzetti 2001; Leccardi & Molendi 2008). Our estimates of σ_V and T_X are fully consistent when assuming the equipartition of energy density between ICM and galaxies. We obtain $\beta_{spec} = 1.09^{+0.18}_{-0.15}$ to

be compared with $\beta_{\rm spec} = 1$, where $\beta_{\rm spec} = \sigma_{\rm V}^2/(kT/\mu m_{\rm p})$ with $\mu = 0.58$ the mean molecular weight and $m_{\rm p}$ the proton mass (see also Fig. 6). Taking this result at face value one might think that A2294 is not far from dynamical equilibrium and the virial mass estimate $M(<R_{\rm vir} \sim 3\ h_{70}^{-1}$ Mpc) $\sim 4 \times 10^{15}\ h_{70}^{-1}\ M_\odot$ computed in Sect. 3.2 to be quite reliable.

5.1. Internal structure

However, our analysis indicates that this cluster is not so relaxed as one may interpret at first glance. Evidence of this comes from both optical and X-ray analyses.

First of all, both the integral and differential velocity dispersion profiles rise in the central region out to $\sim 0.2\ h_{70}^{-1}$ Mpc (Fig. 6, middle and bottom panels). As for the velocity dispersion, this behavior might be a signature of a relaxed cluster exhibiting circular velocities and galaxy merger phenomena in the central cluster region (e.g., Merritt 1988; Menci & Fusco Femiano 1996; Girardi et al. 1998). Alternatively, it might be the signature of subclumps of different mean velocities (see, e.g., Abell 3391–3395 in Girardi et al. 1996; Abell 115 in Barrena et al. 2007b). The latter hypothesis is supported by the behavior of the mean velocity profile and by the plot of velocity versus projected clustercentric distance, where the central region is more populated by low velocity galaxies than high velocity galaxies. This suggests the presence of substructure in the cluster core.

Second, the two gaps found in the velocity distribution indicate that there are three subclumps with the BCG in the middle velocity subclump. Although the presence of the three groups (GV1, GV2, GV3) is not very strongly significant on the basis of only velocity data, the existence of a spatial segregation between GV1 and GV3 groups is a indicator of true substructures. We also find a (marginally significant) velocity gradient toward the SSW direction.

Third, the high-luminosity galaxy subsample shows two peaks (largely overlapping) in the velocity distribution, with the BCG being somewhere in-between. This result is very interesting, implying that galaxies of different luminosity may trace the dynamics of cluster mergers in a different way. A noticeable example was reported by Biviano et al. (1996): they found that the two central dominant galaxies of the Coma cluster are surrounded by luminous galaxies, accompanied by the two main X-ray peaks, while the distribution of faint galaxies does not appear to be centered on one of the two dominant galaxies, but is rather coincident with a secondary peak detected in the X-ray image. Biviano et al. speculate that the merging of Coma is in an advanced phase, where faint galaxies trace the forming structure of the cluster, while the most luminous galaxies still trace the remnant of the core-halo structure of a pre-merging clump, which may be sufficiently dense to survive for a long time after the merging (as suggested by numerical simulations, e.g. González-Casado et al. 1994). In A2294, luminous galaxies may trace the remnants of two merging subclusters characterized by an impact velocity $\sim$2000 km s^{-1}. Assuming the dynamical equilibrium for each of the two individual subclusters, from the values of $\sigma_{\rm V}$ of the two subclusters we obtain a virial mass of $1.8 \times 10^{15}\ h_{70}^{-1}\ M_\odot$ and $0.5 \times 10^{15}\ h_{70}^{-1}\ M_\odot$ for the low and high velocity subclusters. The total mass $M_{\rm sys} = 2.3 \times 10^{15}\ h_{70}^{-1}\ M_\odot$ is lower than the global virial value computed in Sect. 3.2, but is still a high value.

As for the X-ray data, we find no evidence of obvious substructure. Our multiscale wavelet analysis of the Chandra image does not identify any subclumps in the X-ray photon distribution. We also confirm the absence of a significant, macroscopic cluster ellipticity (see also Hashimoto et al. 2007; Maughan et al. 2008).

As for the Beta model we fit, the value of the core radius $R_{\rm c} = 104.4^{+7.7}_{-7.3}\ h_{70}^{-1}$ kpc and the value of the slope parameter $\beta_{\rm fit,\,gas} = 0.49 \pm 0.03$ agree well with those computed by Hart in his PhD thesis (2008; $R_{\rm c} = (99 \pm 12)\ h_{70}^{-1}$ kpc; $\beta_{\rm fit,\,gas} = 0.48 \pm 0.02$). The value of the core radius agrees with that expected from the relation between surface brightness concentration index and core radius shown by Hashimoto et al. (2007, see their Fig. 8 and the value of concentration in their Table 2). The values of $R_{\rm c}$ and $\beta_{\rm fit,\,gas}$ lie on the low end of the parabolic relation found between these two parameters (Neumann & Arnaud 1999). On the other hand, the value of $\beta_{\rm fit,\,gas} = 0.49 \pm 0.03$ might be somewhat small compared to the typical values for very rich/hot clusters (e.g., Jones & Forman 1999; Vikhlinin et al. 1999). However, we note that most of our signal comes from the region with a radius of $\sim 0.5\ h_{70}^{-1}$ Mpc ($\sim 1/6\, R_{\rm vir}$) and that there are indications of a continuous steepening of the X-ray brightness profiles with increasing radius (e.g., Vikhlinin et al. 1999; Neumann 2005). This steepening is the most likely cause of offsets between different cluster samples (see Vikhlinin et al. 1999 where $\beta_{\rm fit,\,gas} \gtrsim 0.6$ vs. Jones & Forman 1999 where $\left\langle \beta_{\rm fit,\,gas} \right\rangle = 0.6$) and of apparent discrepancies between fit parameters obtained for the same clusters (e.g. Buote et al. 2005). Indeed, the most appropriate way to compare different clusters it seems is to consider the measure of the local slope of the surface brightness at a certain, rescaled radius (see Croston et al. 2008 for variation of this parameter with radius). As for A2294, Maughan et al. (2008) computed the slope $\beta_{500} = 1.22^{+0.32}_{-0.25}$ at a radius of $R_{500} = 1.3\ h_{70}^{-1}$ Mpc, using the data in the radial range $0.7R_{500}$–$1.3R_{500}$, i.e. well outside the region we analyze. This value is in agreement with that expected for very hot clusters at $z < 0.5$ (see their Fig. 11). Finally, we note that, in the case of a cluster merger, numerical simulations predict a clear expansion of the gas core and a steepening of the slope (Roettiger et al. 1996, see their Fig. 3). This agrees with the results of Jones & Forman (1999) to explain the large core radii found for a few observed clusters, but we refer to Neumann & Arnaud (1999) for no link between $\beta_{\rm fit,gas}$ value and cluster dynamical status. To summarize, our small values of $R_{\rm c}$ and $\beta_{\rm fit,gas}$ are not indicative of substructure. Direct evidence of cluster substructure comes from the 2D image of the Beta model residuals, which shows positive residuals in the X-ray emission along the SE–NW direction (see Fig. 12).

To interpret the residual image, we simulate two systems, both having an X-ray surface brightness profile following a Beta model with the same $\beta_{\rm fit,\,gas}$, but different $R_{\rm c}$ and S_0, with the centers separated by a distance of the order of the two adopted core radii. The surface brightness profile of the composed system has a single peak, as in the case of A2294 (see Fig. 14, upper panel). The fit with a single Beta model provides a value for $R_{\rm c} \sim 50\%$ and $\sim$20% larger than the two adopted core radii, respectively. Instead, $\beta_{\rm fit,\,gas}$ is $\sim$10% larger than the adopted value. The appearance of the 2D image of the residuals (Fig. 14, lower panel) is roughly similar to that obtained for A2294, with a two-clump surplus of X-ray photons (with the left clump being the most evident) in the line defined by the centers of the subsystems and a deficit in the perpendicular direction (cf. Fig. 14 with Fig. 12). Thus the residual image of A2294 data might be explained by two very close (or very closely projected) systems along the SE–NW direction. In particular, we find that an asymmetry between

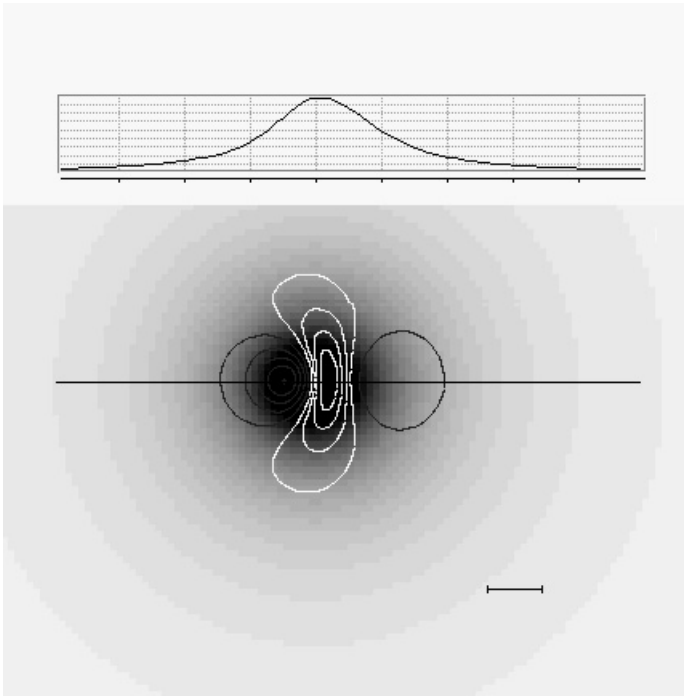

Fig. 14. *Upper panel*: integrated X-ray profile of the simulated system composed of two subsystems, both following a Beta model profile but with different model parameters (see text). *Lower panel*: surface brightness distribution of the simulated system with, superimposed, the contour levels of the Beta model residuals. White (dark/gray) contours represent negative (positive) residuals. As a reference, the size of the fitted core radius is drawn.

the two components might explain the more prominent excess of the SE structure in the residual image. Some pieces of observational evidence found in the literature, i.e. the presence of a centroid shift (Rizza et al. 1998; Maughan et al. 2008, but see Hashimoto et al. 2007) or a certain degree of asymmetry of the X-ray profile around the centroid of the photon distribution (Hashimoto et al. 2007) are likely to be connected with the substructure we detect. Our above bimodal model is obviously a very simplified scenario in the case of a close interaction between two galaxy systems – as we discuss below – and we do not attempt to go further in interpreting the observed data, e.g., exploring in more detail the quantitative parameters.

5.2. Investigating the likely merger cluster

The absence of a macroscopic elongation of the galaxy and ICM distributions and the poor significance of the velocity gradient suggests that the evidence of substructure we detect is a trace of minor/old accretion phenomena or that the direction of the cluster merger is aligned along the LOS. The LOS direction might explain the difficulty of the analysis of the cluster internal dynamics. Another example of a cluster merger along the LOS is the galaxy cluster CL 0024+17, an apparently relaxed system, which is actually a collision between two clusters, the interaction occurring along our LOS, as demonstrated by Czoske et al. (2002) using about 300 galaxies with redshifts in the cluster field.

The cluster merger scenario is generally consistent with the absence of the cool core. Although simulations yield ambivalent results about the role of mergers in destroying cool cores (Poole et al. 2006; Burns et al. 2008), observations seem to favor cool core destruction by means of cluster mergers (Allen et al. 2001; Sanderson et al. 2006). In particular, the LOS merging direction might explain the high compactness of A2294 with respect to other non-cool core clusters (Bauer et al. 2005, see their Fig. 3). We note that our new data for the BCG exclude the presence of Hα emission, which had been previously reported by Crawford et al. (1995), thus reclassifying A2294 as a quite "normal" non-cool core.

In the framework of a cluster merger where the two subclusters are well traced by the luminous galaxies (for the non-collisional part, i.e., dark matter and galaxies) and the residual image (for the collisional part, i.e., the gas), we may also obtain some information about the evolutionary stage of the merger. Assuming that $\beta_{\rm spec} = 1$ for each of the two subclusters, from the values of σ_V we obtain the X-ray temperatures $T_{\rm X} = 7.0$ and 2.8 keV. The observed X-ray temperature is thus ~1.4 times that of the main subcluster. While the observed X-ray temperature of the merging simulated clusters is still not clear at later times (e.g. 2–3 Gyr after the collision, see ZuHone et al. 2009 and refs. therein), numerical simulations agree in finding enhancements of the X-ray temperature around the time of the core-crossing. After a very sharp rise, the temperature peaks either during the core-crossing or just after and then declines (Ricker & Sarazin 2001; Mastropietro & Burkert 2008). Since we see no evidence of a very hot, arc-shaped feature at the cluster center, we assume that the merger is being captured after the core-crossing, i.e. during the outgoing phase. For the case of a 1:3 mass ratio, Fig. 8 of Ricker & Sarazin (2001) suggests a time $\lesssim$0.5 Gyr after the core-crossing.

At this point, we have the minimum amount of observation-based information to be able to apply the two-body model (Beers et al. 1982; Thompson 1982) following the methodology outlined for, e.g., Abell 1240 (Barrena et al. 2009). This simple model assumes radial orbits for the clumps with no shear or net rotation of the system. According to the boundary conditions usually considered, the clumps are assumed to begin their evolution at time $t_0 = 0$ with a separation $d_0 = 0$, and are now moving apart or coming together for the first time in their history. In the case of a collision, we assume that the time $t_0 = 0$ with separation $d_0 = 0$ is the time of their core-crossing and that we are looking at the system after a time t. The values of the relevant parameters for the two-subcluster system are: $t \sim 0.5$ Gyr, the relative LOS velocity in the rest-frame, $V_{\rm rf} \sim 2000$ km s^{-1}, and the projected linear distance between the two clumps, $D \sim 0.1\ h_{70}^{-1}$ Mpc. The last parameter is deduced from the residual image and therefore might be an underestimate of the non-collisional component.

The bimodal model solution gives the total system mass $M_{\rm sys}$, i.e. the sum of the masses of the two subclusters, as a function of α, where α is the projection angle between the plane of the sky and the line connecting the centers of the two clumps (e.g., Gregory & Thompson 1984). Figure 15 compares the bimodal-model solutions with the observed mass of the system $M_{\rm sys} = 2.3 \times 10^{15}\ h_{70}^{-1}\ M_{\odot}$ considering a 50% uncertainty band. Among other solutions, we find the bound outgoing solution (BO) with $\alpha \sim 85°$, i.e. the cluster merger is occurring largely in the LOS direction, in agreement with our expectations. In the framework of this solution the SE clump, which is the more X-ray luminous and thus probably the more massive, is moving towards SE in the direction of the observer, while the less X-ray luminous and massive NW subcluster is moving towards NW in the opposite direction with respect to the observer. The true spatial distance between the two subclumps is $D_{\rm 3D} \sim 1\ h_{70}^{-1}$ Mpc and the real, i.e. deprojected, velocity

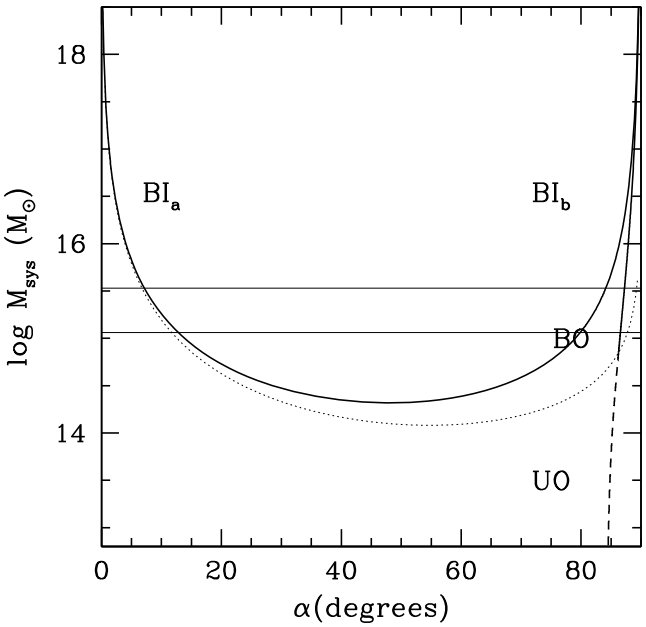

Fig. 15. System mass vs. projection angle for bound and unbound solutions (thick solid and thick dashed curves, respectively) of the two-body model applied to the low and high velocity subclusters. Labels BI_a and BI_b indicate the bound and incoming, i.e., collapsing solutions (thick solid curve). Label BO indicates the bound outgoing, i.e., expanding solutions (thick solid curve). Label UO indicates the unbound outgoing solutions (thick dashed curve). The horizontal lines give the range of observational values of the mass system with a 50% error. The thin dashed curve separates bound and unbound regions according to the Newtonian criterion (above and below the thin dashed curve, respectively).

difference is $V_{rf,3D} \sim 2000$ km s^{-1}. In this scenario, we expect the presence of a gas shock (Bykov et al. 2008, and refs. therein). We can estimate the Mach number of the shock to be $\mathcal{M} = v_s/c_s$, where v_s is the velocity of the shock and c_s is the sound speed in the pre-shock gas (see e.g., Sarazin 2002 for a review). The value of c_s can be obtained from our estimate of $\sigma_V \sim 1070$ km s^{-1} for the most massive subcluster. For the value of v_s, we use $v_s \gtrsim V_{rf,3D} = 2000$ km s^{-1}, since after the core crossing the shock velocity is larger than the subcluster velocity (see Fig. 4 of Springel & Farrar 2007 and Fig. 14 of Mastropietro & Burkert 2008). This leads to $\mathcal{M} \gtrsim 2$, in agreement with the moderate Mach numbers $2 \leq \mathcal{M} \leq 4$ expected for shocks due to the cluster merging.

In conclusion, present observational evidence is consistent with A2294 being a very massive cluster that has just formed or is in the process of forming by means of a merger, i.e. similar to most DARC clusters we previously analyzed (e.g. Boschin et al. 2006; Barrena et al. 2007a; Girardi et al. 2008). The timescale of a few fractions of Gyr agrees both with the results of other merging clusters showing radio halos/relics (e.g., Markevitch et al. 2002; Girardi et al. 2008; Barrena et al. 2009) and with theoretical expectations for radio halos (Brunetti et al. 2009). The morphology of the A2294 radio halo is somewhat intriguing. After the subtraction of discrete sources, the radio halo of A2294 appears quite elongated along the EW direction as shown by Giovannini et al. (2009; their Fig. 10 on the left), while the radio halos of other DARC clusters have either a round structure or a structure elongated in the direction of the merger (Abell 697, Girardi et al. 2006; Abell 520, Girardi et al. 2008). This appearent misalignment with the projected merging direction (SE–NW) deserves further investigation.

In general, to verify our hypothesis of a cluster merger in A2294 and more accurately quantify the merging framework we suggest both the acquisition of many more redshifts in the cluster field and/or deeper X-ray observations. In particular, deeper X-ray data would allow us to confirm the temporal phase of the merger, although the LOS geometry of the merger implies that the direct observation of the shock would be difficult (e.g., Markevitch et al. 2005). The acquisition of more redshifts might allow us to more accurately determine the non-collisional components of the merging subclusters.

Acknowledgements. We are in debt with Gabriele Giovannini for the VLA radio image and his useful comments. M.G. acknowledges financial support from ASI-INAF I/088/06/0 grant. We thank the anonymous referee for his/her very stimulating suggestions. This publication is based on observations made on the island of La Palma with the Italian Telescopio Nazionale Galileo (TNG) and the Isaac Newton Telescope (INT). The TNG is operated by the Fundación Galileo Galilei – INAF (Istituto Nazionale di Astrofisica). The INT is operated by the Isaac Newton Group. Both telescopes are located in the Spanish Observatorio of the Roque de Los Muchachos of the Instituto de Astrofisica de Canarias. This research has made use of the NASA/IPAC Extragalactic Database (NED), which is operated by the Jet Propulsion Laboratory, California Institute of Technology, under contract with the National Aeronautics and Space Administration.

References

Abell, G. O., Corwin, H. G. Jr., & Olowin, R. P. 1989, ApJS, 70, 1
Allen, S. W., Ettori, S., & Fabian, A. C. 2001, MNRAS, 324, 877
Ashman, K. M., Bird, C. M., & Zepf, S. E. 1994, AJ, 108, 2348
Bardelli, S., Zucca, E., Vettolani, G., et al. 1994, MNRAS, 267, 665
Barrena, R., Boschin, W., Girardi, M., & Spolaor, M. 2007a, A&A, 467, 37
Barrena, R., Boschin, W., Girardi, M., & Spolaor, M. 2007b, A&A, 469, 861
Barrena, R., Girardi, M., Boschin, & Dasí, M. 2009, A&A, 503, 357
Bauer, F. E., Fabian, A. C., Sanders, J. S., Allen, S. W., & Johnstone, R. M. 2005, MNRAS, 359, 1481
Beers, T. C., Geller, M. J., & Huchra, J. P. 1982, ApJ, 257, 23
Beers, T. C., Flynn, K., & Gebhardt, K. 1990, AJ, 100, 32
Beers, T. C., Forman, W., Huchra, J. P., Jones, C., & Gebhardt, K. 1991, AJ, 102, 1581
Beers, T. C., Gebhardt, K., Huchra, J. P., et al. 1992, ApJ, 400, 410
Bertin, E., & Arnouts, S. 1996, A&AS, 117, 393
Bird, C. M., & Beers, T. C., 1993, AJ, 105, 1596
Biviano, A., Durret, F., Gerbal, D., et al. 1996, A&A, 311, 95
Biviano, A., Girardi, M., Giuricin, G., Mardirossian, F., & Mezzetti, M. 1992, ApJ, 396, 35
Biviano, A., Katgert, P., Mazure, A., et al. 1997, A&A, 321, 84
Boschin, W., Girardi, M., Barrena, R., et al. 2004, A&A, 416, 839
Boschin, W., Girardi, M., Spolaor, M., & Barrena, R. 2006, A&A, 449, 461
Brunetti, G., Cassano, R., Dolag, K., & Setti, G. 2009, A&A, 507, 661
Boschin, W., Barrena, R., Girardi, M., & Spolaor, M. 2008, A&A, 487, 33
Buote, D. A. 2002, in Merging Processes in Galaxy Clusters, ed. L. Feretti, I. M. Gioia, & G. Giovannini (The Netherlands: Kluwer Ac. Pub.) Optcial Analysis of Cluster Mergers
Buote, D. A., Humphrey, P. J., & Stocke, T. 2005, ApJ, 630, 750
Burns, J. O., Hallman, E. J., Gantner, B., Motl, P. M., & Norman, M. L. 2008, ApJ, 675, 1125
Burstein, D., & Heiles, C. 1982, AJ, 87, 1165
Bykov, A. M., Dolag, K., & Durret, F. 2008, Space Sci. Rev., 134, 119
Carlberg, R. G., Yee, H. K. C., & Ellingson, E. 1997, ApJ, 478, 462
Cash, W. 1979, ApJ, 228, 939
Cassano, R., & Brunetti, G. 2005, MNRAS, 357, 1313
Cassano, R., Brunetti, G., Röttgering, H. J. A., & Brüggen, M. 2010, A&A, 509, A68
Cavaliere, A., & Fusco-Femiano, R. 1976, A&A, 49, 137
Cousins, A. W. J. 1976, Mem. R. Astr. Soc, 81, 25
Crawford, C. S., Edge, A. C., Fabian, A. C., et al. 1995, MNRAS, 274, 75
Croston, J. H., Pratt, G. W., Böhringer, et al. 2008, A&A, 431, 443
Czoske, O., Moore, B., Kneib, J.-P., & Soucail, G. 2002, A&A, 386, 31
Danese, L., De Zotti, C., & di Tullio, G. 1980, A&A, 82, 322
Dickey, J. M., & Lockman, F. J. 1990, ARA&A, 28, 215
Dressler, A., & Shectman, S. A. 1988, AJ, 95, 985
Ebeling, H., Edge, A. C., Böhringer, H., et al. 1998, MNRAS, 301, 881

Edwards, L. O. V., Hudson, M. J., Balogh, M. L., & Smith, R. J. 2007, MNRAS, 379, 100
Ellingson, E., & Yee, H. K. C. 1994, ApJS, 92, 33
Ensslin, T. A., Biermann, P. L., Klein, U., & Kohle, S. 1998, A&A, 332, 395
Ensslin, T. A., & Gopal-Krishna 2001, A&A, 366, 26
Fadda, D., Girardi, M., Giuricin, G., Mardirossian, F., & Mezzetti, M. 1996, ApJ, 473, 670
Feretti, L. 1999, MPE Report No. 271
Feretti, L. 2002a, The Universe at Low Radio Frequencies, Proceedings of IAU Symposium 199, held 30 Nov–4 Dec 1999, Pune, India, ed. A. Pramesh Rao, G. Swarup, & Gopal-Krishna, 2002., 133
Feretti, L. 2005, X-Ray and Radio Connections, ed. L. O. Sjouwerman, & K. K. Dyer. Published electronically by NRAO, http://www.aoc.nrao.edu/events/xraydio. Held 3–6 February 2004 in Santa Fe, New Mexico, USA
Feretti, L. 2006, Proceedings of the XLIst Rencontres de Moriond, XXVIth Astrophysics Moriond Meeting: From dark halos to light, ed. L. Tresse, S. Maurogordato, & J. Tran Thanh Van, [astro-ph/0612185]
Feretti, L. 2008, Mem. SAIt, 79, 176
Feretti, L., Gioia I. M., & Giovannini G. 2002b, Astrophysics and Space Science Library, Merging Processes in Galaxy Clusters (The Netherlands: Kluwer Academic Publisher), 272
Ferrari, C., Govoni, F., Schindler, S., Bykov, A. M., & Rephaeli, Y. 2008, Space Sci. Rev., 134, 93
Fusco-Femiano, R., & Menci, N. 1998, ApJ, 498, 95
Giovannini, G., Bonafede, A., Feretti, L., et al. 2009, A&A, 507, 1257
Giovannini, G., & Feretti, L. 2002, in Merging Processes in Galaxy Clusters, ed. L. Feretti, I. M. Gioia, & G. Giovannini (The Netherlands: Kluwer Ac. Pub.): Diffuse Radio Sources and Cluster Mergers
Giovannini, G., Tordi, M., & Feretti, L. 1999, New Astron., 4, 141
Girardi, M., & Mezzetti, M. 2001, ApJ, 548, 79
Girardi, M., & Biviano, A. 2002, in Merging Processes in Galaxy Clusters, ed. L. Feretti, I. M. Gioia, & G. Giovannini (The Netherlands: Kluwer Ac. Pub.): Optical Analysis of Cluster Mergers
Girardi, M., Fadda, D., Giuricin, G., et al. 1996, ApJ, 457, 61
Girardi, M., Giuricin, G., Mardirossian, F., Mezzetti, M., & Boschin, W. 1998, ApJ, 505, 74
Girardi, M., Boschin, W., & Barrena, R. 2006, A&A, 455, 45
Girardi, M., Barrena, R., & Boschin, W. 2007, Contribution to Tracing Cosmic Evolution with Clusters of Galaxies: Six Years Later, conference – http://www.si.inaf.it/sesto2007/contributions/Girardi.pdf
Girardi, M., Barrena, R., Boschin, W., & Ellingson, E. 2008, A&A, 491, 379
Goto, T. 2005, MNRAS, 359, 141
González-Casado, G., Mamon, G. A., & Salvador-Solé, E. 1994, ApJ, 433, 61
Gregory, S. A., & Thompson, L. A. 1984, ApJ, 286, 422
Gullixson, C. A. 1992, in Astronomical CCD Observing and Reduction techniques, ed. S. B. Howell, ASP Conf. Ser., 23, 130
Hart, B. C. 2008, Evolution of substructure in galaxy clusters as observed in X-rays, PhDT [arXiv:0801.4093]
Hashimoto, Y., Böhringer, H., Henry, J. P., Hasinger, G., & Szokoly, G. 2007, A&A, 467, 485
Hoeft, M., Brüggen, M., & Yepes, G. 2004, MNRAS, 347, 389
Johnson, H. L., & Morgan, W. W. 1953, ApJ, 117, 313
Jones, C., & Forman, W. 1999, ApJ, 511, 65
Kempner, J. C., Blanton, E. L., Clarke, T. E. et al. 2004, Proceedings of the conference, The Riddle of Cooling Flows in Galaxies and Clusters of Galaxies, ed. T. H. Reiprich, J. C. Kempner, & N. Soker, [astro-ph/0310263]
Kennicutt, R. C. 1992, ApJS, 79, 225
Landolt, A. U. 1992, AJ, 104, 340
Leccardi, A., & Molendi, S. 2008, A&A, 486, 359
Limber, D. N., & Mathews, W. G. 1960, ApJ, 132, 286
López-Cruz, O., Barkhouse, W. A., & Yee, H. K. C. 2004, ApJ, 614, 679
Malumuth, E. M., Kriss, G. A., Dixon, W. V. D., Ferguson, H. C., & Ritchie, C. 1992, AJ, 104, 495
Markevitch, M., Gonzalez, A. H., David, L., et al. 2002, ApJ, 567, 27
Markevitch, M., Govoni, F., Brunetti, G, & Jerius, D. 2005, ApJ, 627, 733
Mastropietro, C., & Burkert, A. 2008, MNRAS, 389, 967
Maughan, B. J., Jones, C., Forman, W., & Van Speybroeck, L. 2008, ApJS, 174, 117
Merritt, D. 1988, in The Minneosota lectures on clusters of galaxies and large-scale structure (A90–36758 15–90). San Francisco, CA, Astronomical Society of the Pacific, 1988, 175
Menci, N., & Fusco-Femiano, R. 1996, ApJ, 472, 46
Mushotzky, R. F., & Scharf, C. A. 1997, ApJ, 482, L13
NAG Fortran Workstation Handbook, 1986 (Downers Grove, IL: Numerical Algorithms Group)
Neumann, D. M., & Arnaud, M. 1999, A&A, 348, 711
Neumann, D. M., & Arnaud, M. 2005, A&A, 439, 465
Ota, N., Pointecouteau, E., Hattori, M., & Mitsuda, K. 2004, ApJ, 601, 1200
Owen, F., Morrison, G., & Voges, W. 1999, proceedings of the workshop, Diffuse Thermal and Relativistic Plasma in Galaxy Clusters, ed. H. Böhringer, L. Feretti, & P. Schuecker, MPE Report 271, 9
Peres, C. B, Fabian, A. C., Edge, A. C., et al. 1998, MNRAS, 298, 416
Pisani, A. 1993, MNRAS, 265, 706
Pisani, A. 1996, MNRAS, 278, 697
Poggianti, B. M. 1997, A&AS, 122, 399
Poole, G. B., Fardal, M. A., Babul, A., et al. 2006, MNRAS, 373, 881
Press, W. H., Teukolsky, S. A., Vetterling, W. T., & Flannery, B. P. 1992, in Numerical Recipes 2nd edn. (Cambridge University Press)
Quintana, H., Carrasco, E. R., & Reisenegger, A. 2000, AJ, 120, 511
Raymond, J. C., & Smith, B. W. 1977, ApJS, 35, 419
Ricker, P. M., & Sarazin, C. L. 2001, ApJ, 561, 621
Rizza, E., Burns, J. O., Ledlow, M. J., et al. 1998, MNRAS, 301, 328
Rizza, E., Morrison, G. E., Owen, F. N., et al. 2003, AJ, 126, 119
Roettiger, K., Burns, J. O., & Loken, C. 1996, ApJ, 473, 651
Roettiger, K., Loken, C., & Burns, J. O. 1997, ApJS, 109, 307
Roettiger, K., Burns, J. O., & Stone, J. M. 1999, ApJ, 518, 603
Sanderson, A. J. R., Ponman, T. J., & O'Sullivan, E. 2006, MNRAS, 372, 1496
Sarazin, C. L. 2002, in Merging Processes in Galaxy Clusters, ed. L. Feretti, I. M. Gioia, & G. Giovannini (The Netherlands: Kluwer Ac. Pub.): The Physics of Cluster Mergers
Springel, V., & Farrar, G. R. 2007, MNRAS, 380, 911
The, L. S., & White, S. D. M. 1986, AJ, 92, 1248
Thompson, L. A. 1982, in Early Evolution of the Universe and the Present Structure, ed. G.O. Abell, & G. Chincarini (Dordrecht: Reidel), IAU Symposium, 104
Tonry, J., & Davis, M. 1979, ApJ, 84, 1511
Tribble, P. C. 1993, MNRAS, 261, 57
Vikhlinin, A., Forman, W., & Jones, C. 1999, ApJ, 525, 47
Wainer, H., & Schacht, S. 1978, Psychometrika, 43, 203
ZuHone, J. A., Ricker, P. M., Lamb, D. Q., & Karen Yang, H.-Y. 2009, ApJ, 699, 1004